On the dynamics of an observed thermal front off central eastern Australia

Peter R. Oke,[1] Matthew H. England, and Jason H. Middleton

Centre for Environmental Modeling and Prediction, School of Mathematics, University of New South Wales, Sydney, New South Wales, Australia

Received 1 March 2002; revised 25 July 2002; accepted 16 September 2002; published 2 April 2003.

[1] Results from a short observational program off central eastern Australia (28.4°S) are presented. A series of events involving sharp temperature fluctuations and strong pulses in the alongshore currents are measured by a mooring array over the inner shelf. With use of AVHRR images, ADCP, and CTD surveys, it is reasoned that these events correspond to the periodic advection of a thermal front past the inshore moorings. The front involves a temperature change of 1°–2°C, with a southward jet of greater than 0.5 m s^{-1} over a width of 1–2 km in 25 m of water. The dynamical balances of the momentum equations are examined. It is demonstrated that at the onset of each event the local tendency of alongshore velocity is balanced by across-shore advection. Additionally, a quasi-balance between the surface and bottom stress terms is noted throughout the experiment demonstrating the prominence of mixing over the inner shelf. *INDEX TERMS:* 4528 Oceanography: Physical: Fronts and jets; 4512 Oceanography: Physical: Currents; 4576 Oceanography: Physical: Western boundary currents; *KEYWORDS:* fronts, upwelling, momentum balance, coastal circulation, inner-shelf circulation

Citation: Oke, P. R., M. H. England, and J. H. Middleton, On the dynamics of an observed thermal front off central eastern Australia, *J. Geophys. Res.*, *108*(C4), 3106, doi:10.1029/2002JC001370, 2003.

1. Introduction

[2] Thermal fronts have been observed on numerous occasions in the East Australian Current (EAC) region [e.g., *Rochford*, 1975; *Godfrey et al.*, 1980; *Cresswell et al.*, 1983; *Tranter et al.*, 1986; *Roughan and Middleton*, 2002]. These fronts have involved temperature changes of up to 5°C [e.g., *Rochford*, 1975; *Tranter et al.*, 1986; *Roughan and Middleton*, 2002]. Some of these observations have been in the vicinity of Cape Byron [e.g., *Godfrey et al.*, 1980], the location of the field program described here, where a sharp front has been observed to separate colder water near the coast and warmer water offshore. Using remotely sensed measurements, *Cresswell et al.* [1983] observed a thermal front that was associated with the separation of the EAC from the coast, reporting that the oceanic conditions on the shoreward (colder) side of the front were very turbulent, with the appearance of "confused breaking waves". *Tranter et al.* [1986] observed several fronts from remotely sensed data that were associated with the separation of the EAC from the coast, noting that high levels of Chlorophyll were associated with these fronts. The importance of thermal fronts as biological indicators is well established [e.g., *Washburn et al.*, 1991; *Franks and Walstad*, 1997].

[3] Although fronts are known to be common features of the inner shelf (here defined as within 5 km of the coast) in the EAC region, in situ measurements of such fronts are rare, and so their detailed structure remains unknown. For example, details of these fronts that remain unclear include the magnitude of the temperature gradient across the fronts, the strength of the currents associated with the fronts, whether the fronts are surface-to-bottom, how the fronts are formed and advected, and what dominant dynamical balances exist in the vicinity of the front. Each of these issues is addressed in this study through an analysis of measurements obtained during a short, intensive field program off central eastern Australia at 28.4°S during October 1996.

[4] The outline of this paper is as follows. A description of the observational program is presented in section 2, followed by observations of a thermal front in section 3 and details of the genesis and evolution of the front in section 4. An analysis of the dynamical balances in the vicinity of the front is presented in section 5 followed by a summary in section 6.

2. Data Acquisition

[5] The field program was conducted in October 1996 off central eastern Australia at 28.4°S (Figure 1). A shore-normal array of current meters and thermistors was deployed for a period of twelve days commencing on 7 October. The focus of this study is on the three day period between 16–19 October. The instrumentation was deployed on moorings over the inner shelf, midshelf and shelf break as indicated in Figure 1. Here, we focus on the inner shelf array that consists of three, closely spaced moorings between the depths of 25 and 32 m. Reference is also made

[1]Now at CSIRO Marine Research, Hobart, Tasmania, Australia.

0148-0227/03/2002JC001370$09.00

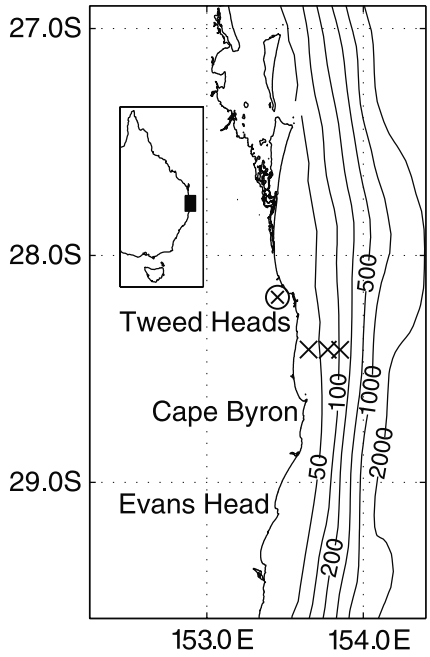

Figure 1. Experiment location showing the mooring positions (crosses) and the location of wind measurements (circled crosses). Moorings A–C are near the mooring position closest to shore, mooring D is over the midshelf near the 50 m isobath, and moorings E and F are over the shelf break near the 100 m isobath.

to measurements over the midshelf in 60 m of water and the shelf break in 95 m of water. The details of the instrumentation that are utilized in this study are presented in Table 1. The current meters measure horizontal velocity vectors with components (u, v) in the (x, y) directions where x and y denote the across-shore and alongshore directions respectively. The thermistors measure temperature T at five minute intervals.

[6] Additionally, we consider measurements from two Acoustic Doppler Current Profiler (ADCP) surveys, one conductivity-temperature-depth (CTD) survey and two advanced very high resolution radiometry (AVHRR) images obtained from the NOAA-11 satellite. These data are used to put the detailed analysis of the measurements from the inshore moorings into the context of the general circulation on the shelf at the time of the experiment. Finally, wind measurements are obtained from a location approximately 31.5 km to the north of the experiment site as denoted in Figure 1, giving the across-shore and alongshore components of wind stress, τ^{Sx} and τ^{Sy} respectively.

3. Observations of the Front

[7] AVHRR images for 11 and 16 October are presented in Figure 2, showing a temperature change of over 2°C between the inner shelf and midshelf moorings. From these images this front appears to separate 20°C water near the coast and water that is warmer than 22°C offshore over 1 or 2 pixels, where the resolution of the AVHRR images is approximately 1.1 km. Additionally, the image on 11 October shows a cold-core, cyclonic meander located to the north and offshore of the mooring array. This meander is not evident in the 16 October image, however the region where we expect the meander is located (directly offshore of the mooring array) is partially hidden by clouds.

[8] The time series of observed winds, temperatures at mooring A, alongshore and across-shore currents at moorings B and C, and across-shore currents at mooring D are shown in Figure 3. On 16 October there is a reversal in the alongshore flow at moorings B and C that is presumably associated with the cyclonic meander that is evident in the AVHRR images (Figure 2). Following 16 October there is a series of upwelling-favorable wind pulses, during which time the temperature at mooring A decreases from approximately 20°C to about 17.5°C over 2.5 days.

[9] Of particular interest for this study is the series of fluctuations in temperature and alongshore currents at the inshore moorings, denoted in Figure 3 as E1–E4. These fluctuations involve sharp temperature increases and strong southward pulses in the alongshore currents. Prior to each event E1–E3 the across-shore currents at 15 m depth at mooring D and at 10 m depth at mooring C are directed onshore (Figures 3d and 3e). We suggest that the fluctuations at the inshore moorings are related to the periodic across-shore advection of a thermal front with colder water on the shoreward side and warmer water offshore. The presence of a front is confirmed by the temperature section obtained during the CTD survey (Figure 4) showing a temperature change of over 1°C over a distance of approximately 1 km shoreward of moorings A and B. Interestingly, the lens of warm water that penetrates to the bottom at station 2 is suggestive of convergence at the front. The timing of the start of the CTD section coincides with a peak in temperature at mooring A (Figure 3b, the CTD survey started near the coast). We suggest that the temperature peaks denote the times when the thermal front is closest to the coast. At the start of the CTD survey, the front may have extended inshore of the first CTD station.

[10] By the thermal wind relation,

$$v_z = -g\rho_x(\rho_0 f)^{-1}, \tag{1}$$

where v_z is the vertical shear of the alongshore current, ρ_x is the across-shore gradient of density, g is gravity, ρ_0 is a background density and f is the Coriolis parameter, we expect the velocity field associated with the front to involve a vertically sheared southward flow. Although we cannot determine the vertical profile of the alongshore flow from the inshore moorings, the strong southward pulses are consistent with the presence of a narrow jet passing by the moorings. Additionally, the alongshore velocity fields in the two ADCP sections (Figure 5) show evidence of a very

Table 1. Details of the Instrumentation and Mooring Array That Are Considered in This Study

Mooring	Instrument Type	Depth, m	Water Depth, m	Offshore Distance, km
A	3 thermistors	10, 15, and 20	25	1.05
B	1 current meter	10	25	1.1
C	1 current meter	10	32	1.9
D	2 current meters	15 and 55	60	12.1
E	1 thermistor	90	95	21.5
F	2 current meters	10 and 90	95	21.55

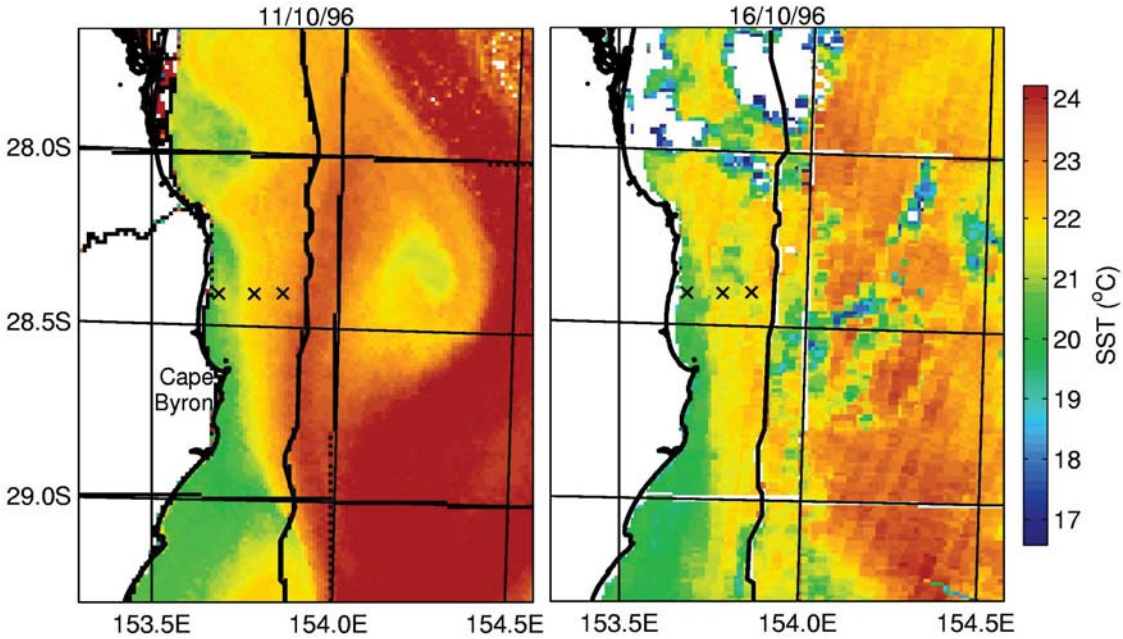

Figure 2. AVHRR images of SST for (left) 11 and (right) 16 October. The inshore, midshelf, and shelf break mooring locations are denoted by crosses; the 300 m isobath is shown.

narrow southward jet in the vicinity of moorings B and C prior to event E1. Although the ADCP measurements do not extend to the surface, the alongshore velocity fields suggest a surface intensified southward jet. The vertical shear v_z in the upper part of the water column near the jet in the ADCP survey is approximately -0.013 s^{-1}. In about the same location, the horizontal density gradient between CTD stations 2 and 3 is approximately -1.05×10^{-4} kg m^{-4}, which corresponds to a right hand side of (1) of -0.014 s^{-1}. This shows that the thermal wind relation is valid around the jet indicating that the dominant balance in the across-shore momentum equation (discussed in section 5) is geostrophic.

[11] The horizontal resolution of the processed ADCP data is approximately 0.5 km, and the ADCP fields show the jet width as narrow as 1–2 km. This is consistent with the observations from moorings B and C that are located less than 1 km apart. The southward pulse at mooring C precedes the pulse at mooring B, and by the time the pulse occurs at mooring B, the alongshore velocity at mooring C is already weakening. Given the separation between these moorings, we conclude that the jet has a half-width of less than 1 km at 10 m depth.

[12] The fluctuations measured at moorings A, B and C that are associated with events E1–E4 occur first at mooring C (located 2 km offshore), closely followed by mooring B (located 1.1 km offshore) and then at mooring A (located 1 km offshore). This sequence of events is consistent with the onshore advection of a front. However, curiously the reverse sequence to that described above does not occur when across-shore currents are positive (i.e., when we would expect to see the front advected offshore). We suggest three possible explanations for this. Firstly, the onshore advection may act to intensify the front, while offshore advection may weaken it. Secondly, mixing inshore of the moorings may result in entrainment of colder water, resulting in the erosion of the front. Thirdly, the fluctuations may simply be associated with internal waves. The analyses of the dominant dynamical balances in section 5 support the feasibility of the first two explanations. In contrast, an analysis of the velocity components at the inshore mooring in the frequency domain shows that the components at the relevant frequencies are not in quadrature. This demonstrates that the fluctuations at the inshore moorings are not simply associated with a progressive internal wave. Additionally, the temperature change during each event involves a temperature increase, rather than an alternate decrease and increase that is expected to be associated with an internal wave.

[13] The temperature fluctuations at 10 m depth at mooring A during events E1–E4 suggest that the temperature change across the front is between 1 and 2°C and the AVHRR images show the temperature change to be over 2°C at the surface (Figure 2). Consideration of the lag time between the fluctuations at moorings A, B and C suggests that the speed of advection of the front between the inshore moorings is between 0.09 and 0.13 m s^{-1}. Comparison of the temperature fluctuations at the top and bottom of mooring A shows that the front is not vertical. This is consistent with the CTD section (Figure 4).

[14] The salient features of the observations described above are summarized in Figure 6, showing a schematic diagram of the thermal front and the associated jet. The analysis that follows attempts to identify the processes that cause the formation, maintenance and across-shore advection of the front (section 4), and to determine the nature of the dominant dynamical balances associated with the front (section 5).

4. Genesis and Evolution of the Front

[15] Insight into the processes that cause the front to be advected across-shore is gained by considering the frequency of the events. Because each of these events occurs

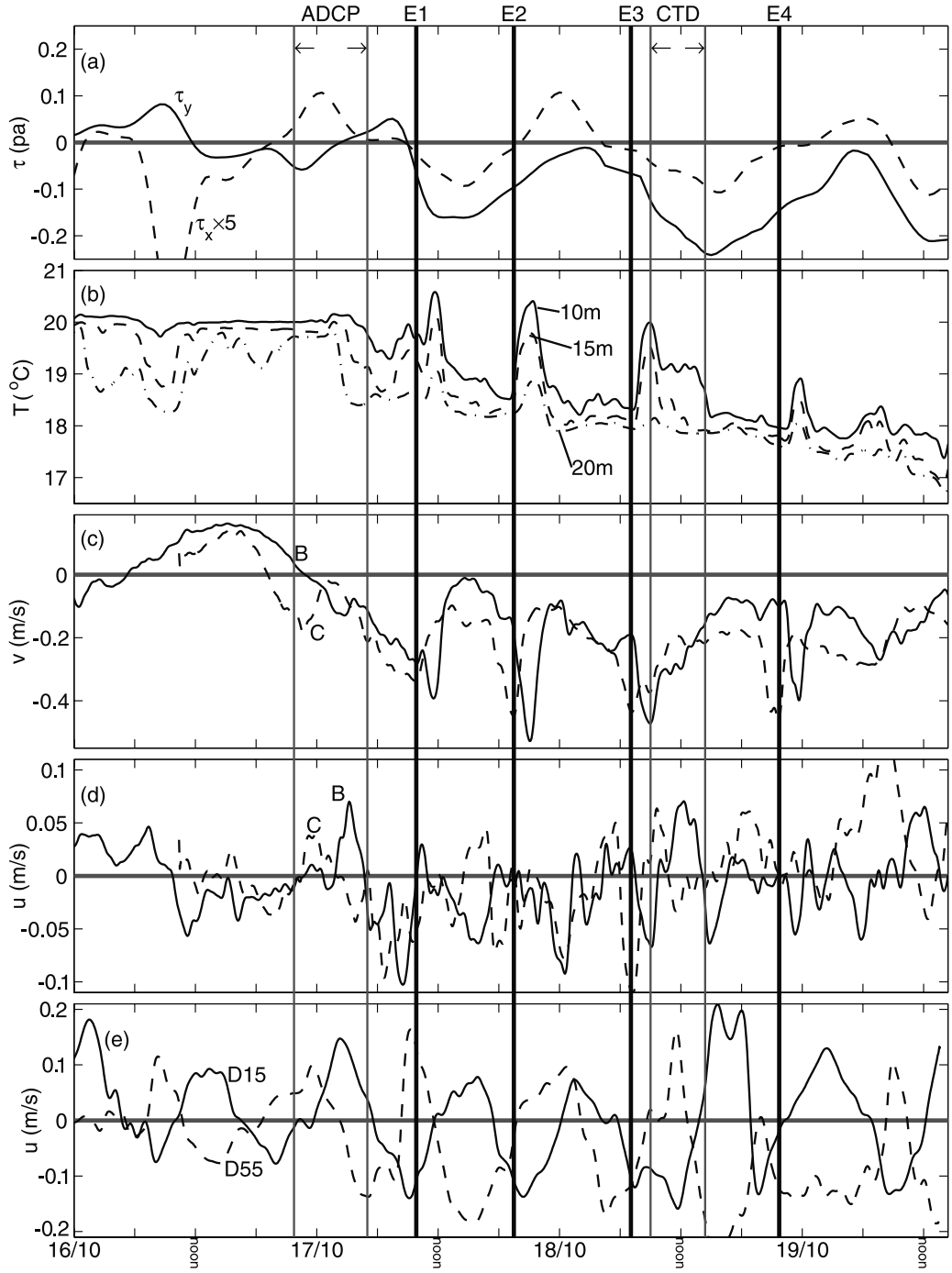

Figure 3. Time series of (a) alongshore (solid) and across-shore (dashed, multiplied by 5) wind stress τ^S; (b) temperature T, from mooring A at depths of 10 m (solid), 15 m (dashed) and 20 m (dashed-dotted); (c) alongshore velocity v, and (d) across-shore velocity u, from mooring B (solid) and C (dashed) at 10 m depth; and (e) across-shore velocity from mooring D at 15 m (solid) and 55 m (dashed) depth. The four frontal events, labeled E1–E4, corresponding to the peaks in v at mooring C are denoted by the bold vertical lines and the start and end of the ADCP and CTD surveys are denoted by the shaded vertical lines.

approximately 12 hours apart, the semidiurnal tide is the most obvious candidate. Notably, the across-shore currents at 15 m depth at mooring D and at mooring C are directed onshore prior to each event E1–E3 (Figures 3d and 3e). The amplitude of the semidiurnal across-shore currents at 15 m depth at mooring D are between 0.1 and 0.2 m s^{-1} (Figure 3e). Additionally, during this period the semi-diurnal across-shore currents at the top and bottom of mooring D appear to be out of phase. Indeed, the cross-correlations between the 15 m and 55 m across-shore currents at mooring D for the period of interest is −0.58. This is a key characteristic of baroclinic, or internal tides [e.g., *Petruncio et al.*, 1998].

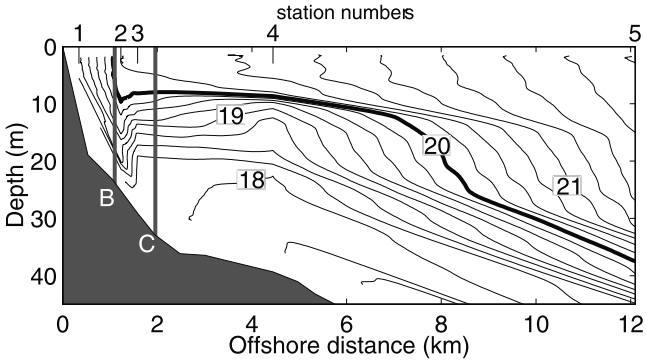

Figure 4. Across-shore temperature section from the CTD survey performed between 9:00 am and 2:45 pm on 18 October. The station locations are labeled above the plot, and the locations of moorings B and C are indicated.

Another characteristic of internal tides is that their associated currents are typically surface and bottom intensified. We therefore suggest that the strong across-shore currents associated with the semi-diurnal internal tide are effective at advecting the front, and its associated jet, across the shelf periodically. The details noted in section 2 demonstrate that, in contrast, the inshore fluctuations are not related to an internal wave. Thus while the large amplitude tidal currents affect the inshore circulation, the baroclinic nature of the tidal currents is attenuated between the midshelf and inshore moorings. The reason why the events are not precisely 12 hours apart is due to the influence of processes other than tides, such as wind-forcing and fluctuations in the EAC.

[16] As noted in section 1 there is evidence of convergence at the front (Figure 4). Notably, the semidiurnal signals at moorings B and C are less clear than at mooring D. Furthermore, the semidiurnal signals at moorings B and C do not appear to covary. Perhaps the semidiurnal tidal signal is becoming so attenuated toward the coast that across-shore convergence of tidal currents is playing a role in the development of the front.

[17] One aspect of the front that is of interest is the mechanism by which the front is formed. An AVHRR image on 5 October (not shown), taken before the start of the observation program, shows the front already present in the vicinity of the mooring array. Consequently, we cannot address the formation mechanism of the front using our observation array. However, the persistence of the front over this extended period demonstrates that the front can survive a range of different conditions.

[18] Other aspects of interest are those processes that contribute to the maintenance of the front. It is possible that the front is a wind-driven upwelling front. As noted above, the period covering events E1–E4 coincides with upwelling-favorable winds. However, the initial event E1 represents a temperature increase, rather than a decrease as would be associated with upwelling. This temperature increase during E1 suggests that warmer water (probably associated with the EAC) may have shifted toward the coast. Therefore, it is possible that the EAC is playing a role in the maintenance of the front. In support of this, the ADCP sections show strong southward currents over the midshelf that may be associated with the EAC. Additionally, the numerical investigations of *Oke and Middleton* [2000, 2001] and the observations of *Roughan and Middleton* [2002] showed that when the EAC is in close proximity to the shelf, persistent current-driven upwelling can result. The importance of the EAC and local wind-forcing during our observed record is addressed below.

[19] Time series of low-pass filtered alongshore wind stress, currents from the bottom of moorings D and F and temperature from the bottom of moorings A, D and E are shown for the whole experimental period in Figure 7. The bottom-most instruments from moorings D, E and F are approximately 5 m off the bottom and therefore provide the best available estimate of flow fields in the bottom boundary layer. The approximate times of the zero-crossing of the alongshore wind stress and the across-shore currents at the bottom of moorings D and F for the upwelling events that begin on 9 and 16 October are denoted in Figure 7. Clearly, the shift to upwelling-favorable winds leads the shift to onshore currents at the bottom of moorings D and F. Similarly, the timing of the temperature decrease at moorings A, D and E lag the shift to upwelling-favorable winds. This suggests that these upwelling events are primarily wind driven.

[20] A complicating factor here is the apparent intrusion of the EAC prior to 10 October. This intrusion is evident in the 4°C temperature increase at the bottom of mooring E (Figure 7d) and the acceleration of the alongshore currents at the top of mooring F (Figure 7e). The temperature increase is interpreted as an EAC intrusion since an identifying feature of the EAC is that it transports warm water southwards. It is possible that the intrusion of the EAC

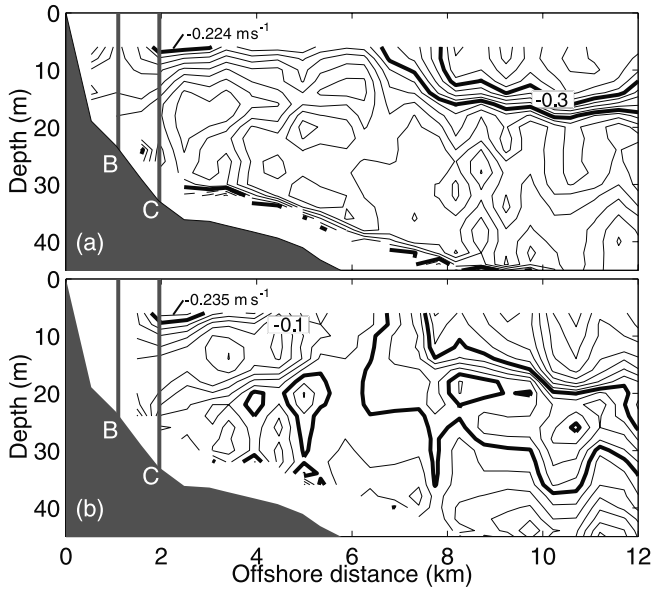

Figure 5. Across-shore sections of alongshore velocity measured from ADCP surveys between (a) 9:45 pm on 16 October and 1:00 am on 17 October and (b) 1:40 am and 5:00 pm on 17 October. The contour interval is 0.025 m s^{-1}, the zero, -0.2 and -0.3 m s^{1} contours are thick lines, negative (southward) contours are solid lines and positive (northward) contours are dashed lines. The locations of moorings B and C and the maxima of the inshore jet are indicated.

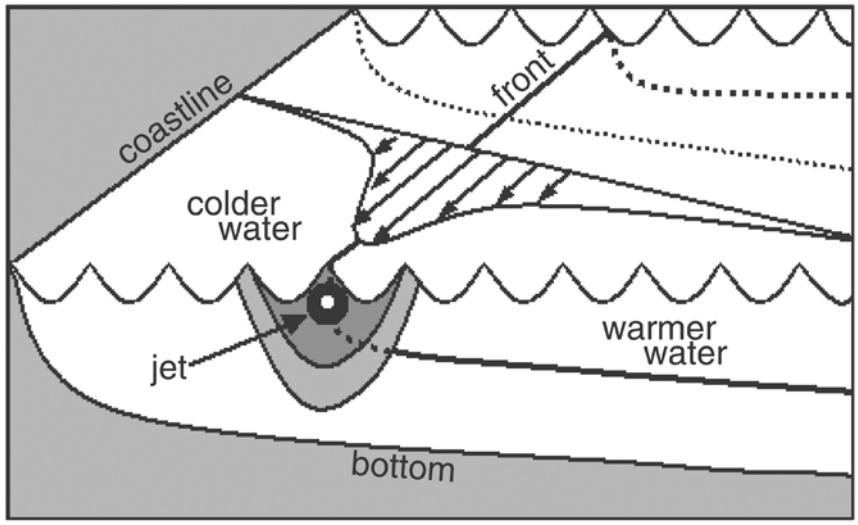

Figure 6. Schematic diagram of the thermal front and associated alongshore jet.

generates a current-driven bottom boundary layer that may be contributing to the observed upwelling. Equally, however, the temperature decrease at mooring E (after the EAC intrusion subsides) may simply be due to the offshore movement of the warm EAC water. However, the presence of onshore currents at the bottom of mooring F appear contrary to this suggestion. There is no apparent EAC intrusion prior to the upwelling event that begins on 16 October. Whether EAC-driven upwelling plays some role remains uncertain, however it is clear that wind-driven upwelling is dominant during the observed upwellings.

[21] Regardless of the mechanisms at work, the upwelling events have the potential to transport colder water across the shelf and onto the inner shelf. This is clearly evident in the temperature records. The time integral of the across-shore currents at the bottom of moorings D and F are also shown in Figure 7f. This represents the potential horizontal distance over which the across-shore currents may advect water. The close agreement between these time integrals suggests that the bottom boundary layer flow is fairly continuous across the entire shelf. During the upwelling events that begin on 9 and 16 October the potential horizontal distance over which the near-bottom across-shore currents may advect isotherms is up to 28 and 12 km respectively. Even if the opposing buoyancy forces reduce this displacement by 50%, this is sufficient to uplift water from the midshelf to the coast, or from the shelf break to the midshelf. These events are likely to contribute to the maintenance of the observed front over the inner shelf.

5. Momentum Balances

[22] The depth-averaged across-shore and alongshore momentum equations are given by

$$U_t + UU_x + VU_y - fV + \left(\tau^{Bx} - \tau^{Sx}\right)/(\rho_0 H) + P_x/\rho_0 = 0 \quad (2)$$

and

$$V_t + UV_x + VV_y + fU + \left(\tau^{By} - \tau^{Sy}\right)/(\rho_0 H) + P_y/\rho_0 = 0 \quad (3)$$

respectively, where U and V are the depth-averaged alongshore and across-shore velocities respectively, $f = -6.92 \times 10^{-5}$ s^{-1} is the Coriolis parameter at 28.4°S, $\rho_0 = 1023$ kg m^{-3} is a reference density, H is the local water depth; τ^{Sx} and τ^{Sy} are the across-shore and alongshore components of surface stress respectively; τ^{Bx} and τ^{By} are the across-shore alongshore components of bottom stress respectively; P is pressure and subscripts x, y and t denote partial derivatives with respect to the across-shore direction, the alongshore direction and time respectively.

[23] Not all of the terms in (2) and (3) can be calculated directly from the data because of the limited observations. As a result, several assumptions are made in an attempt to close the momentum budget represented by (2) and (3). Central to this analysis is the assumption that the measured velocity at 10 m depth is equivalent to the depth-averaged velocity. The only available measurements of the velocity profile over depth in the vicinity of the inshore moorings are from the ADCP surveys (Figure 5). Profiles of alongshore velocity, averaged over 1.5 km horizontally centered on the narrow, southward jet approximately 2.5 km offshore, are plotted in Figure 8. The estimated depth-averaged velocity for these profiles is also plotted. For these limited examples, the alongshore velocity at 10 m depth is approximately equal to the depth-averaged velocity, supporting the assumption that the observed velocity is an appropriate substitute for the depth-averaged velocity. Alternatively, one could consider the depth-dependent versions of (2) and (3), however, this introduces vertical viscosity terms that involve second order derivatives in the vertical direction. Again, without multiple measurements over depth, these terms cannot be estimated directly from the mooring array. Conveniently, the depth-average of the vertical viscosity terms are simply the sum of the surface and bottom stress terms. For example,

$$\int_{-H}^{0} (K_M v_z)_z dz = \left(\tau^{Sy} - \tau^{By}\right)/(\rho_0), \quad (4)$$

where K_M is a vertical viscosity coefficient that is normally considered to be flow-dependent in modeling studies [e.g.,

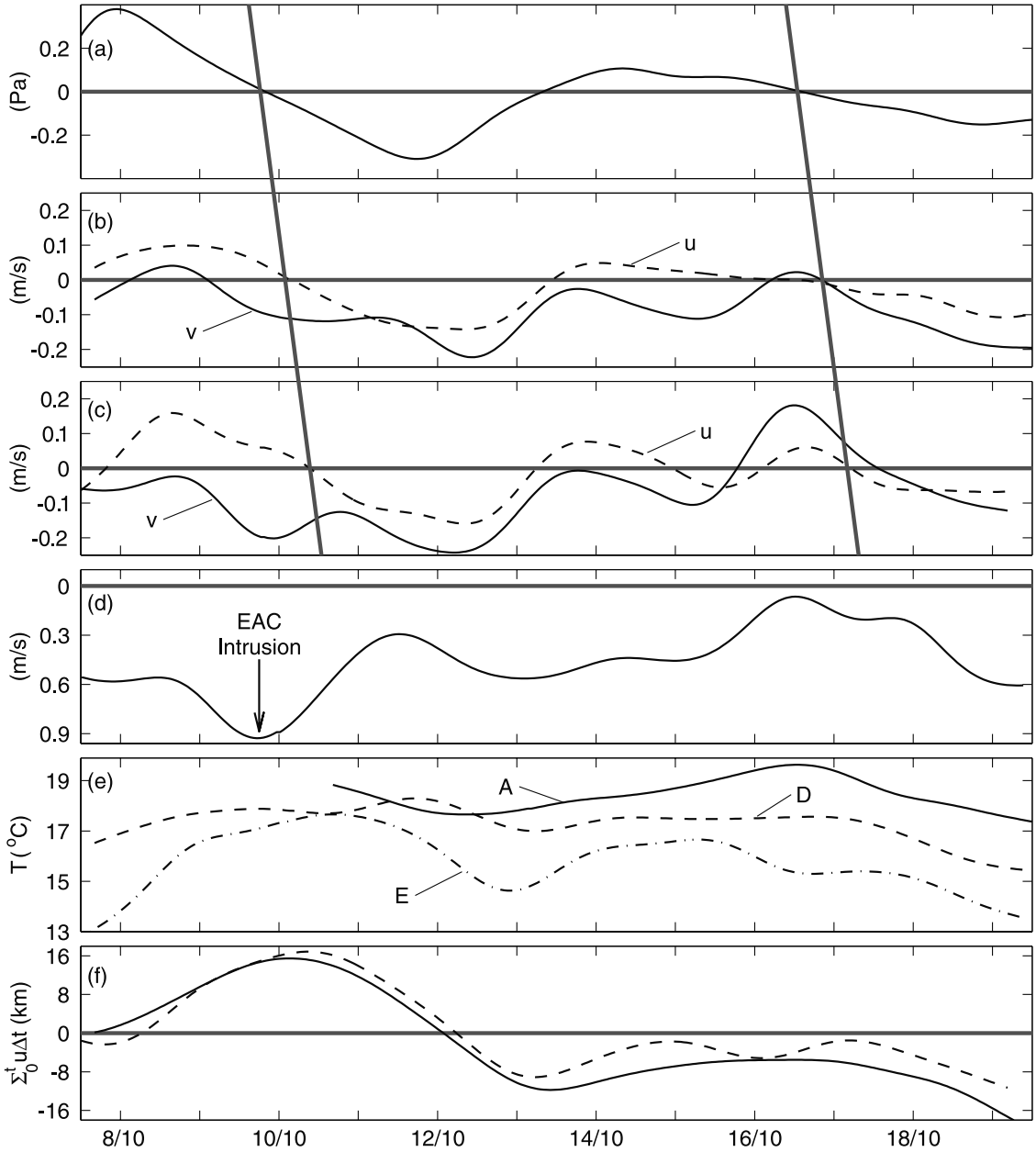

Figure 7. Time series of the low-pass filtered (a) τ^{Sy}, (b) u (dashed) and v (solid) at the bottom of mooring D, (c) u and v at the bottom of mooring F, (d) v at the top of mooring F, (e) T at the bottom of moorings A, D and E, and (e) the time integral of the across-shore currents $\Sigma_0^t u\Delta t$, from the bottom of moorings D (solid) and F (dashed). The slanted shaded lines denote the approximate reversal times of τ^{Sy} and u at moorings D and F.

Mellor and Yamada, 1982]. Additionally, the bottom stress term is simplified by adopting a linear drag law,

$$\left(\tau^{Bx}, \tau^{By}\right)/(\rho_0 H) = \left(u^B, v^B\right) r/H, \tag{5}$$

where the superscript B denotes bottom, and $r = 5 \times 10^{-4}$ m s^{-1}, based on previous observations [e.g., *Lentz and Winant*, 1986], is the linear bottom friction coefficient. Since the bottom velocity is not measured here, we will assume that the bottom velocity (at 25 m depth) is proportional to the measured velocity (at 10 m depth). This is expected if the dominant fluctuations are barotropic. We expect the measured velocity to be stronger than the true bottom velocity, although an appropriate scaling constant is not clear from the profiles presented in Figure 8. This difference in magnitude could be accounted for by simply adjusting r [*Lentz et al.*, 1999], however, this introduces subjectivity into the analysis and so we have not implemented any such adjustments here. Unfortunately, we are unable to calculate the across-shore pressure gradient term in (2) because of insufficient pressure and density measurements. Additionally, we cannot estimate terms involving alongshore gradients. We therefore have to assume that the terms involving U_y, V_y and P_y are small. This is partially justified

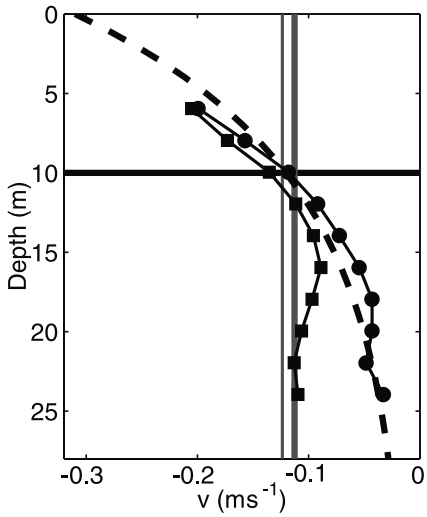

Figure 8. Average profiles of alongshore velocity over depth for the first (circles) and second (squares) ADCP survey presented in Figure 5. The averages are over 1.5 km in the across-shore direction, centered 2 km offshore. The dashed line is an exponential fit to the first profile, and the bold vertical line is the depth average of the fitted curve. The thin vertical line is the depth average of the second profile. The 10 m depth is denoted.

by the AVHRR images (Figure 2) that show that near the inshore moorings alongshore gradients in temperature are small compared to across-shore gradients. In an idealized modeling study of the continental shelf circulation in this region, *Oke and Middleton* [2000] showed that alongshore gradients in modeled fields are small adjacent to the coast compared to the midshelf region where, in response to the narrowing of the continental shelf near Cape Byron, the modeled fields vary considerably in the alongshore direction. It should be noted, however, that observational studies in other coastal regions have found the alongshore pressure gradient term to be important [e.g., *Scott and Csanady*, 1976; *Brink et al.*, 1978; *Allen and Smith*, 1981; *Lentz and Winant*, 1986].

[24] Any, or all, of the assumptions outlined above may be inappropriate. In part, justification for these assumptions is sought by demonstrating that the sum of the estimated terms, hereafter referred to as the residual, is small compared to the estimated terms. Where the magnitude of the residual is comparable to the other terms the residual is interpreted as the sum of unestimated terms.

[25] The terms in (2) and (3) are calculated in accordance with the assumptions and limitations outlined above. The details of these calculations are presented in the Appendix. Time series plots of the terms for the 3 day period of interest are shown in Figure 9. These plots demonstrate the complexity of the dynamics near the inshore moorings. Clearly, for (2) the Coriolis term is dominant, and is not balanced by any of the terms estimated here. For (3), a relatively steady,

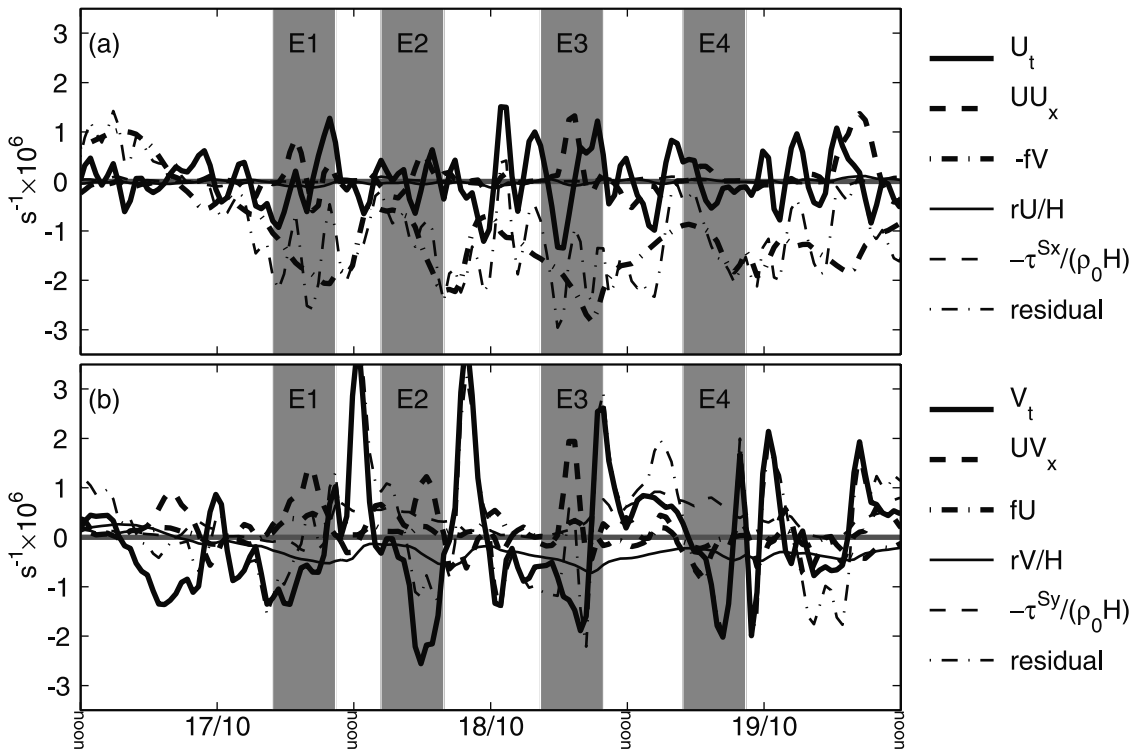

Figure 9. Time series of the terms in (a) the depth-averaged across-shore momentum equation (2) and (b) the depth-averaged alongshore momentum equation (3). A legend is displayed to the right of each plot, and the 6 hour periods preceding the four events E1–E4 analyzed in Figure 12 are highlighted. The residual represents the sum of the pressure gradient term, alongshore advection term and the error.

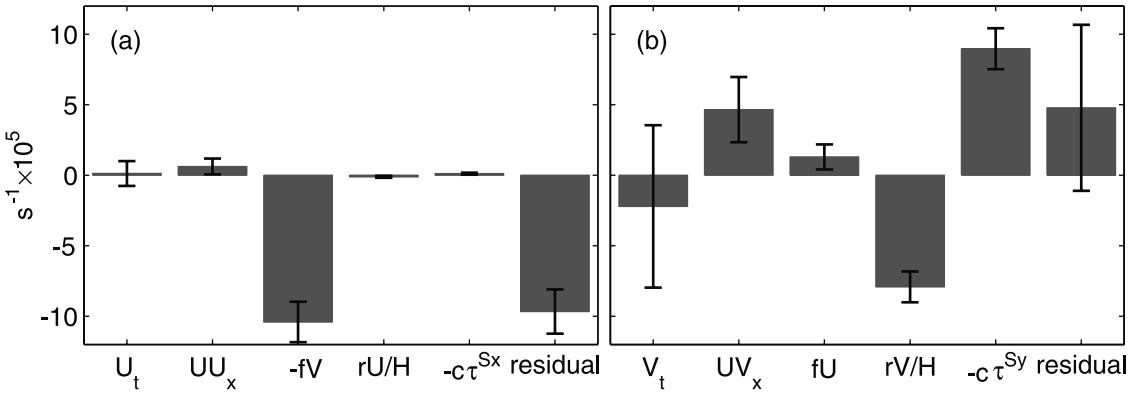

Figure 10. Mean values of terms in (a) the across-shore momentum equation (2) and the (b) alongshore momentum equation equation (3) multiplied by 3, where $c = (\rho_0 H)^{-1}$.

negative bottom stress appears to be balanced by a positive wind stress. Similarly, during events E1–E3 the large negative tendencies that correspond to the southward pulses in the alongshore flow (Figure 3c) appear to be partially balanced by positive across-shore advection. These aspects of the dynamical balances are investigated in more detail below.

[26] The mean values for the terms in (2) and (3) are presented, along with the appropriate standard errors, in Figure 10. Additionally, in order to gain insight into what terms dominate the fluctuations in each equation, the root-mean square (RMS) of every term is presented in Figure 11.

[27] For (2) the large negative Coriolis term in the mean (Figure 10a) is not balanced by any of the estimated terms. Similarly, the dominant terms in the RMS fields for the terms in (2) are the Coriolis and the residual (Figure 11b). Scaling arguments for sub-inertial coastal flow fields with alongshore scales assumed to be greater than across-shore scales imply that, away from the turbulent boundary layers, the alongshore velocity is approximately in geostrophic balance [*Allen and Newberger*, 1996]. We therefore expect the Coriolis term in (2) to be primarily balanced by the across-shore pressure gradient term that could not be estimated here. This is consistent with the calculations of the terms in the thermal wind relation from the ADCP and CTD surveys presented in section 3.

[28] The mean values for (3) demonstrate that there is a balance between the surface and bottom stress terms (Figure 10b). This is not surprising, and is consistent with other coastal regions around the world [e.g., *Allen and Smith*, 1981; *Mitchum and Sturges*, 1982; *Lentz et al.*, 1999; *Oke et al.*, 2002]. Additionally, the tendency term opposes both the advection and Coriolis terms, however, given the prominence of the residual term, the details and significance of the momentum balances of these more minor terms remains unclear.

[29] The RMS of terms in the alongshore momentum equation (3) (Figure 11b) shows that most terms make a significant contribution. The dominant terms are the tendency and residual terms. Again, the prominence of the residual term demonstrates that either the unestimated terms are significant, or that some of our assumptions in calculating the terms may be flawed. In either case, this analysis shows that the RMS of the across-shore advection term in (3) is greater than the surface and bottom stress terms. This implies that local changes in the alongshore velocity near the inshore moorings are more likely to be due to advection rather than external forcing.

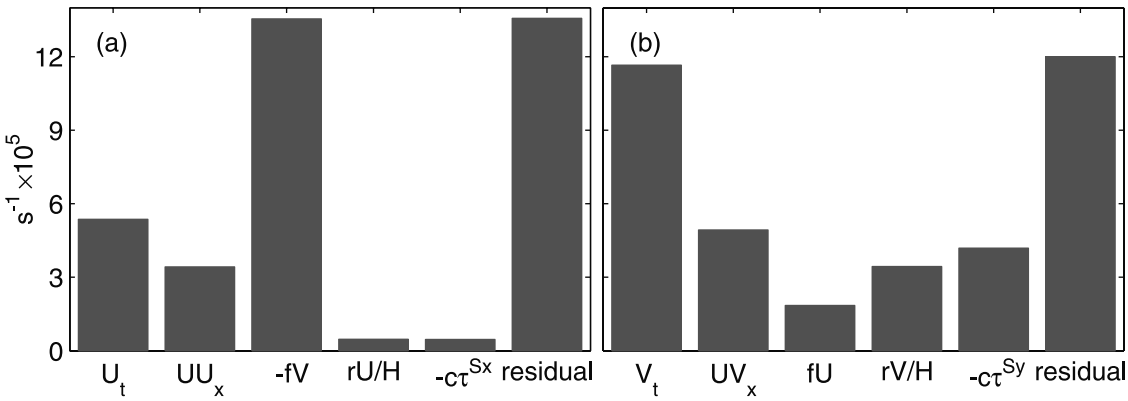

Figure 11. RMS of the terms in (a) the across-shore momentum equation (2) and (b) the alongshore momentum equation (3), where $c = (\rho_0 H)^{-1}$.

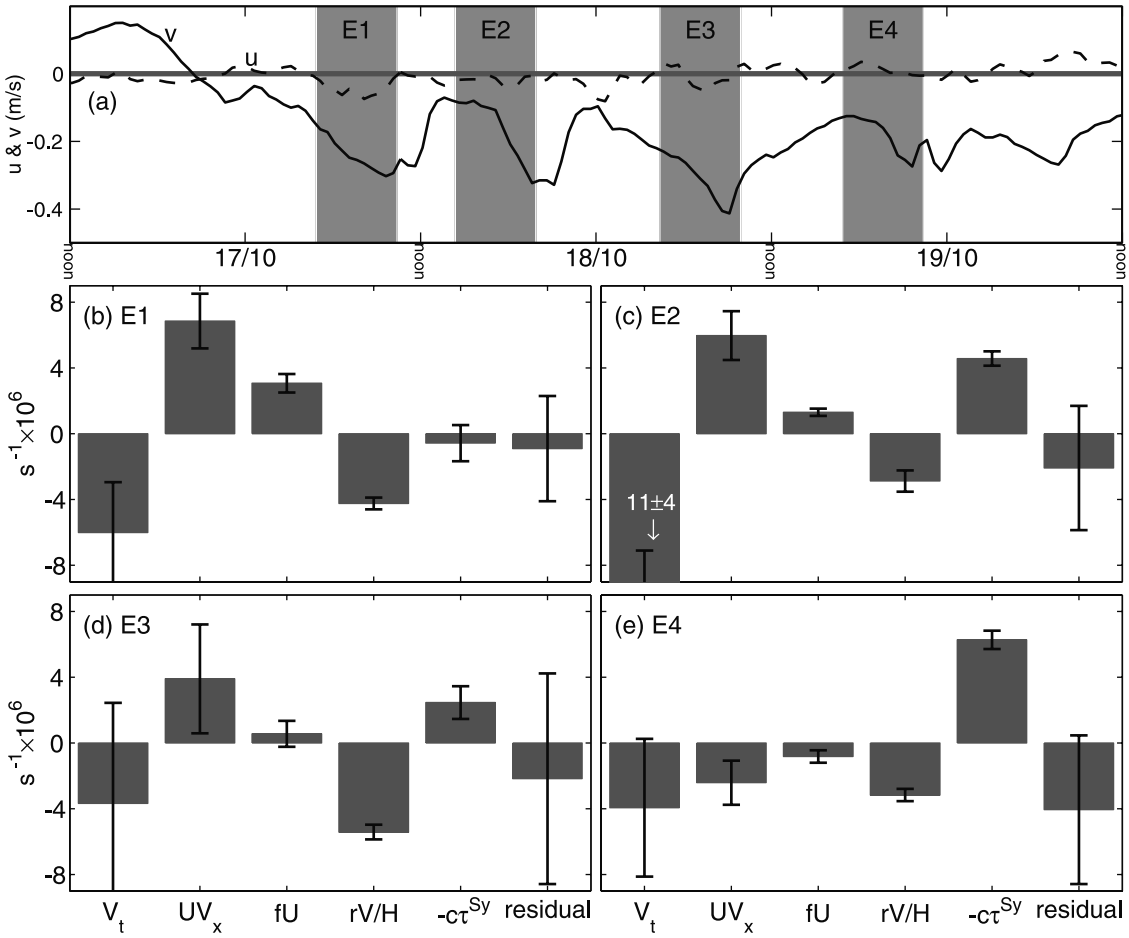

Figure 12. (a) Time series of $\langle u \rangle$ and $\langle v \rangle$ (averaged over the inshore moorings) where the shaded bands denote the 6-hour periods preceding events E1–E4 when the terms in (3) are averaged and presented Figures 12b–12e, respectively. The standard error for each averaged field is shown ($c = (\rho_0 H)^{-1}$).

[30] By focusing on the four events E1–E4 useful information on the dynamical balances in (3) can be extracted. We have averaged the terms in (3) over each six hour period preceding events E1–E4 (Figures 12b–12e). The averaging periods for the events are denoted in Figures 9 and 12a. The averaging period of six hours is chosen because it seems to span the period when the tendency V_t is negative for each event. For events E1–E3 there are four terms with greater magnitudes than the residual (Figures 12b–12d). Despite the standard error of the residual being large, this suggests that during these specific events, the assumptions that are employed to simplify (3) may be reasonable. For event E4, the residual is of comparable magnitude to the other dominant terms. Therefore, we shall focus the discussion that follows on events E1–E3.

[31] For each event E1–E3 a strong negative tendency is primarily balanced by a positive across-shore advection (Figures 12b–12d). During these events the across-shore velocity is weak and negative (onshore flow, Figure 12a). Therefore, since the advection term UV_x is positive, V_x must be negative. This is consistent with the shoreward edge of a southward jet being moved toward the coast (Figure 6).

[32] During each event the bottom stress term has the same sign, and thus opposes the tendency (Figures 12b–12d). Additionally, in E2 and E3 there appears to be a quasi-balance between the surface and bottom stress terms. This is consistent with the mean values for the whole period (Figure 10) and demonstrates the importance of mixing processes over the inner shelf by the relation (4). The time series of temperature in Figure 3b shows that the flow field at mooring A is typically stratified throughout the period of interest. This prompts the question: If mixing is important, why does the flow field remain stratified? We suggest that the effects of surface heating inhibit the water column from becoming vertically well mixed. Close inspection of the temperature time series in Figure 3b shows that T_z is typically large around noon and small around midnight. Thus, during the day a positive surface heat flux increases the stratification, while at night vertical mixing reduces the stratification.

6. Summary

[33] Based on an observational program conducted during October 1996 off central eastern Australia, a description of in situ measurements of a thermal front is presented. It appears that the strong across-shore currents associated with an internal tide over the midshelf periodically advect a thermal front, with an associated southward jet, past an inshore mooring array. The strength of the southward jet is

up to 0.5 m s^{-1} and its width is as little as 1–2 km. The temperature change across the front at 10 m depth is up to 2°C and the average speed of advection of the front between the inshore moorings is approximately 0.11 m s^{-1}.

[34] The nature of the dominant dynamical balances in the momentum equations is examined. It is demonstrated that when the thermal front is advected past the inshore moorings a negative tendency is approximately balanced by across-shore advection in the alongshore depth-averaged momentum equation,

$$V_t + UV_x \approx 0. \tag{6}$$

Additionally, there appears to be an approximate balance between the surface and bottom stress terms, demonstrating the importance of mixing over the inner shelf.

[35] The observations of the thermal front described in this manuscript provide the most comprehensive description of this commonly encountered feature in the EAC region. However, there are certain aspects of these fronts that remain unclear. Specifically, the role of alongshore advection and pressure gradients in the momentum balances has not been resolved by our study. Clearly, more comprehensive field programs, similar to the study described by *Lentz et al.* [1999], are needed to quantify these issues.

Appendix A: Extraction of Terms

[36] The specific terms in (2) are calculated as:

$$U_t \approx (\langle u_{n+1}\rangle - \langle u_{n-1}\rangle)/2\Delta t, \tag{A1}$$

$$UU_x \approx \langle u\rangle \left(u_n^{mC} - u_n^{mB}\right)/\Delta x, \tag{A2}$$

$$-fV \approx -f\langle v_n\rangle, \tag{A3}$$

$$\tau^{Bx}/(\rho_0 H) \approx r\langle u_n\rangle/H, \tag{A4}$$

and similarly for (3), where $\langle u\rangle$ and $\langle v\rangle$ are the across-shore and alongshore velocities averaged over moorings B and C, superscripts *mB* and *mC* refer to measurements from moorings B and C respectively, and subscripts $n-1$, n and $n+1$ refer to the previous, present and next discrete measurement in time respectively. Finally, $\tau^{Sx}/(\rho_0 H)$ is estimated from observed winds, and terms involving pressure and alongshore gradients are not able to be estimated. Prior to these calculations, the five-minute raw data are filtered and sub-sampled to half-hourly data by calculating simple centered averages.

[37] **Acknowledgments.** This research was supported by the Australian Research Council. Thanks are due to G. Nippard for organizing the field trip, and to M. Gibbs, D. Rissik, M. Roughan, I. Suthers and the crew of the Douglas Bede for contributions to the field program.

References

Allen, J. S., and P. A. Newberger, Downwelling circulation on the Oregon continental shelf. Part I: Response to idealized forcing, *J. Phys. Oceanogr.*, *26*, 2011–2035, 1996.

Allen, J. S., and R. L. Smith, On the dynamics of wind-driven shelf currents, *Philos. Trans. R. Soc. London*, *302*, 617–634, 1981.

Brink, D. H., J. S. Allen, and R. L. Smith, A study of low-frequency fluctuations near the Peru coast, *J. Phys. Oceanogr.*, *8*, 1025–1041, 1978.

Cresswell, G. R., C. Ellyett, R. Legeckis, A. F. Pearce, and R. Boyd, Nearshore features of the East Australian Current System, *Aust. J. Mar. Freshwater Res.*, *34*, 105–114, 1983.

Franks, P. J. S., and L. J. Walstad, Phytoplankton patches at fronts: A model of formation and response to wind events, *J. Mar. Res.*, *55*, 1–29, 1997.

Godfrey, J. S., G. R. Cresswell, and F. M. Boland, Observations of low Richardson numbers and undercurrents near a front in the East Australian Current, *J. Appl. Meteorol.*, *10*, 301–307, 1980.

Lentz, S. J., and C. D. Winant, Subinertial currents on the southern California shelf, *J. Phys. Oceanogr.*, *16*, 1737–1750, 1986.

Lentz, S. J., R. T. Guza, S. Elgar, F. Fedderson, and T. H. C. Herbers, Momentum balances on the North Carolina inner shelf, *J. Geophys. Res.*, *104*, 18,205–18,226, 1999.

Mellor, G. L., and T. Yamada, Development of a turbulence closure model for geophysical fluid problems, *Rev. Geophys.*, *20*, 851–875, 1982.

Mitchum, G. T., and W. Sturges, Wind-driven currents on the west Florida straits, *J. Phys. Oceanogr.*, *12*, 1310–1317, 1982.

Oke, P. R., and J. H. Middleton, Topographically induced upwelling off eastern Australia, *J. Phys. Oceanogr.*, *30*, 512–531, 2000.

Oke, P. R., and J. H. Middleton, Nutrient enrichment off Port Stephens: The role of the East Australian Current, *Cont. Shelf Res.*, *21*, 587–606, 2001.

Oke, P. R., J. S. Allen, R. N. Miller, and G. D. Egbert, A modeling study of the three-dimensional continental shelf circulation off Oregon. Part II: Dynamical analysis, *J. Phys. Oceanogr.*, *32*, 1383–1403, 2002.

Petruncio, E. T., L. K. Rosenfeld, and J. D. Paduan, Observations of the internal tide in Monterey Canyon, *J. Phys. Oceanogr.*, *28*, 1873–1902, 1998.

Rochford, D. J., Nutrient enrichment of east Australian coastal waters, II, Laurieton upwelling, *Aust. J. Mar. Freshwater Res.*, *26*, 233–243, 1975.

Roughan, M. M., and J. H. Middleton, A comparison of observed upwelling mechanisms off the east coast of Australia, *Cont. Shelf Res.*, *22*, 2551–2572, 2002.

Scott, J. T., and G. T. Csanady, Nearshore currents off Long Island, *J. Geophys. Res.*, *81*, 5401–5409, 1976.

Tranter, D. J., D. J. Carpenter, and G. S. Leech, The coastal enrichment effects of the East Australian Current eddy field, *Deep Sea Res.*, *33*, 1705–1728, 1986.

Washburn, L., D. C. Kadko, B. H. Jones, T. Hayward, P. M. Kosro, T. P. Stanton, S. Ramp, and T. Cowles, Water mass subduction and the transport of phytoplankton in a coastal upwelling system, *J. Geophys. Res.*, *96*, 14,927–14,945, 1991.

M. H. England and J. H. Middleton, Centre for Environmental Modeling and Prediction, School of Mathematics, University of New South Wales, Sydney, NSW 2052, Australia.

P. R. Oke, CSIRO Marine Research, GPO Box 1538, Hobart, Tasmania 7001, Australia. (peter.oke@csiro.au)